Supplementary Material (ESI) for CrystEngComm
This journal is © The Royal Society of Chemistry

Five naphthalene-amide-bridged Ni(II) complexes: electrochemistry, bifunctional fluorescence responses, removal of contaminants and optimization by CVD

Jing Zhao,[a⊥] Jian Luan,[b⊥] Huixuan Yu,[a] Guocheng Liu,[a*] Hongyan Lin,[a] Xiuli Wang[a*] and Baokuan Chen[c*]

[a] *College of Chemistry and Chemical Engineering, Professional Technology Innovation Center of Liaoning Province for Conversion Materials of Solar Cell, Bohai University, Jinzhou 121013, P. R. China*

[b]*Shenyang National Laboratory for Materials Science, Institute of Metal Research, Chinese Academy of Sciences, Shenyang 110016, P. R. China*

[c]*College of Chemistry, Chemical Engineering and Environmental Engineering, Liaoning Shihua University, Fushun, 113001, P. R.China.*

Materials and characterization

Synthesis of the ligand **L** (*N*,*N*′-bis(pyridin-3-ylmethyl) naphthalene-2,6-dicarboxamide) was previously reported by literature [S1]. All other reagents and solvents for syntheses were purchased from commercial sources and used as received without further purification. FT-IR spectra were obtained using a Varian-640 spectrometer (KBr pellets). Powder X-ray diffraction (PXRD) data were collected with an Ultima IV with D/teX Ultra diffractometer at 40 kV and 40 mA with Cu–$K\alpha$ (λ = 1.5406 Å) radiation radiation over the 2θ range of 5–50°. Thermogravimetric analyses (TGA) were carried out on a Pyris Diamond TG instrument. The morphology and structure of the CNT samples were characterized by scanning electron microscopy (SEM, Nova NanoSEM 430) and high resolution transmission electron microscopy (HRTEM, JEOL2010 at 200 kV). Laser Raman spectroscopy was used to estimate the quality of the CNTs. The specific surface area and pore structure of the samples were investigated with an automatic volumetric sorption analyzer (ASAP 2020 M) using N_2 as the adsorbent at −196 °C. X-ray photo-electron spectroscopy (XPS, Escalab 250, Al Kα). Fluorescence spectra were obtained with a Hitachi F-4500 fluorescence/phosphorescence spectrometer. Electrochemical measurements were performed on a CHI 760E Electrochemical Workstation. UV-Vis absorption spectra were obtained using an SP-1901 UV-Vis spectrophotometer.

X-ray Crystallography

X-ray diffraction data for complexes **1**–**5** were collected on a Bruker SMART APEX II diffractometer equipped with a CCD area detector and graphite-monochromated Mo-Kα (λ =0.71073 Å) with the φ–ω scan technique. All the structures were solved by direct methods and refined anisotropically using the programs SHELXS and SHELXL [S2]. The crystal parameters, data collection, and refinement results are summarized in Table 1 for **1**–**5**. Selected bond distances and bond angles are listed in Tables S1–S5. The CCDC numbers are 1954590–1954594.

Preparation of complexes 1–5 bulk-modified carbon paste electrodes (1–5-CPEs)

A complex **1** bulk-modified carbon paste electrode (**1**-CPE) was fabricated as follows: a mixture containing 0.100 g graphite powder and 0.010 g complex **1** was ground in an agate mortar for approximately 30 min, and then 0.05 mL of paraffin was added with stirring. The homogenized mixture was packed into a 3 mm inner diameter glass tube, and the tube surface was wiped with weighing paper. The electrical contact was established with a copper wire. The same procedure was used for the preparation of **2**–**5**-CPEs.

Synthesis of the CNTs

The surveyed synthesis processes of the CNTs all share the following two common features: Catalysts are typically transition metals (Fe, Co, Ni). These are introduced *via* sublimation or vaporisation of an organometallic precursor. Elements of group 16, such as S, Se or Te are considered essential promoter in CNT growth. Sulfur is supplied *via* sublimation, or in precursors such as thiophene (selenophene or tellurophene for Se and Te) or carbon disulfide *via* vaporisation. Thiophene is preferred in most cases. Thus, we selected complexes **4** and **5** as combined catalyst precursors and promoters for preparing CNTs by the CVD method. The above synthesized complex **4** or **5** (100 mg) powder was placed in a quartz boat inside a quartz tube (diameter 80 mm, length 1000 mm) located in a horizontal electrical furnace. Then the furnace temperature was increased to 800 °C under a argon flow

(300 mL min^{-1}, 99.999% purity) in 40 min, followed by the reduction of the catalyst under a hydrogen atmosphere (200 mL min^{-1}, 99.999% purity) for 60 min. The reactor was then heated to the desired temperature under a argon flow. CNT synthesis was performed under a gas mixture of C_2H_4 (25 mL min^{-1}), Ar (300 mL min^{-1}), and H_2 (200 mL min^{-1}) for 30 min. Following the completion of an experiment, the system was cooled to room temperature under Ar, and black powers of CNT-**4** or CNT-**5** were obtained.

Formation conditions and mechanism of CNT

The CVD strategy to prepare CNTs *in situ* by utilizing Ni-CPs as precursors and metal sources is as follow. Firstly, the furnace was increased to 800 °C under Ar flow, and the Ni-CPs were calcined to NiO nanoclusters. In subsequent heating in a H_2 atmosphere, the NiO nanoclusters were reduced to Ni and aggregated into Ni nanoparticles. Finally, CNTs were grown from these catalyst particles by the CVD of ethylene. The similar strategy is reported by some researchers [S3–S8].

Table S1. Selected bond distances (Å) and angles (°) for complex **1**

Ni(1)–O(1)	2.0570(9)	Ni(1)–O(1W)	2.0923(10)
Ni(1)–O(1)#1	2.0570(9)	Ni(1)–N(1)	2.0998(11)
Ni(1)–O(1W)#1	2.0923(10)	Ni(1)–N(1)#1	2.0998(11)
O(1)–Ni(1)–O(1)#1	180	O(1W)#1–Ni(1)–N(1)	93.13(4)
O(1)–Ni(1)–O(1W)#1	90.93(4)	O(1W)–Ni(1)–N(1)	86.87(4)
O(1)#1–Ni(1)–O(1W)#1	89.07(4)	O(1)–Ni(1)–N(1)#1	89.85(4)
O(1)–Ni(1)–O(1W)	89.07(4)	O(1)#1–Ni(1)–N(1)#1	90.15(4)
O(1)#1–Ni(1)–O(1W)	90.93(4)	O(1W)#1–Ni(1)–N(1)#1	86.87(4)
O(1W)#1–Ni(1)–O(1W)	180	O(1W)–Ni(1)–N(1)#1	93.13(4)
O(1)–Ni(1)–N(1)	90.15(4)	N(1)–Ni(1)–N(1)#1	180.00(5)
O(1)#1–Ni(1)–N(1)	89.85(4)	O(1W)#1–Ni(1)–N(1)	93.13(4)
O(1)–Ni(1)–O(1)#1	180		

Symmetry code: #1 $-x + 1, -y, -z + 1$

Table S2. Selected bond distances (Å) and angles (°) for complex **2**

Ni(1)–O(1)	2.0417(16)	Ni(1)–N(2)	2.0962(19)
Ni(1)–O(3)	2.0523(17)	Ni(1)–O(1W)	2.1158(16)
Ni(1)–N(1)	2.0875(19)	Ni(1)–O(2W)	2.1255(17)
O(1)–Ni(1)–O(3)	177.97(7)	N(1)–Ni(1)–O(1W)	175.99(7)
O(1)–Ni(1)–N(1)	87.97(7)	N(2)–Ni(1)–O(1W)	91.66(7)
O(3)–Ni(1)–N(1)	93.83(7)	O(1)–Ni(1)–O(2W)	90.01(7)
O(1)–Ni(1)–N(2)	91.46(7)	O(3)–Ni(1)–O(2W)	90.96(7)
O(3)–Ni(1)–N(2)	87.56(7)	N(1)–Ni(1)–O(2W)	89.25(7)
N(1)–Ni(1)–N(2)	91.42(8)	N(2)–Ni(1)–O(2W)	178.41(7)
O(1)–Ni(1)–O(1W)	89.38(7)	O(1W)–Ni(1)–O(2W)	87.74(7)
O(3)–Ni(1)–O(1W)	88.87(7)		

Table S3. Selected bond distances (Å) and angles (°) for complex **3**

Ni(1)–N(1)#1	2.070(5)	Ni(1)–O(1)	2.090(4)
Ni(1)–N(1)	2.070(5)	Ni(1)–O(1W)#1	2.100(4)
Ni(1)–O(1)#1	2.090(4)	Ni(1)–O(1W)	2.100(4)
N(1)#1–Ni(1)–N(1)	180.0	O(1)-Ni(1)-O(1W)	90.20(16)
N(1)#1–Ni(1)–O(1)	87.95(16)	O(1)#1-Ni(1)-O(1W)	89.80(16)
N(1)–Ni(1)–O(1)	92.05(16)	N(1)#1-Ni(1)-O(1W)#1	86.74(17)
N(1)#1–Ni(1)–O(1)#1	92.05(16)	N(1)-Ni(1)-O(1W)#1	93.26(17)
N(1)–Ni(1)–O(1)#1	87.95(16)	O(1)-Ni(1)-O(1W)#1	89.80(16)
O(1)–Ni(1)–O(1)#1	180.0	O(1)#1-Ni(1)-O(1W)#1	90.20(16)
N(1)#1-Ni(1)-O(1W)	93.26(17)	O(1W)-Ni(1)-O(1W)#1	180.0
N(1)-Ni(1)-O(1W)	86.74(17)		

Symmetry code: #1 –*x*, –*y* + 2, –*z* + 1

Table S4. Selected bond distances (Å) and angles (^{o}) for complex **4**

Ni(1)–O(1)	2.026(3)	Ni(1)–N(1)	2.104(3)
Ni(1)–O(3)	2.058(3)	Ni(1)–N(2)	2.120(3)
Ni(1)–O(1W)	2.079(3)	Ni(1)–O(2W)	2.128(3)
O(1)–Ni(1)–O(3)	90.19(12)	O(1W)–Ni(1)–N(2)	94.77(12)
O(1)–Ni(1)–O(1W)	172.49(11)	N(1)–Ni(1)–N(2)	93.26(13)
O(3)–Ni(1)–O(1W)	85.62(12)	O(1)–Ni(1)–O(2W)	88.05(11)
O(1)–Ni(1)–N(1)	98.50(12)	O(3)–Ni(1)–O(2W)	83.20(11)
O(3)–Ni(1)–N(1)	94.44(12)	O(1W)–Ni(1)–O(2W)	85.28(11)
O(1W)–Ni(1)–N(1)	88.05(12)	N(1)–Ni(1)–O(2W)	173.07(12)
O(1)–Ni(1)–N(2)	88.55(12)	N(2)–Ni(1)–O(2W)	89.16(12)
O(3)–Ni(1)–N(2)	172.30(12)		

Table S5. Selected bond distances (Å) and angles (^{o}) for complex **5**

Ni(1)–O(1)	2.0502(18)	Ni(1)–N(1)	2.113(2)
Ni(1)–N(3)	2.062(2)	Ni(1)–O(4)#1	2.1536(19)
Ni(1)–O(1W)	2.094(2)	Ni(1)–O(3)#1	2.208(2)
O(1)–Ni(1)–N(3)	94.93(9)	O(1W)–Ni(1)–O(4)#1	86.38(8)
O(1)–Ni(1)–O(1W)	89.37(8)	N(1)–Ni(1)–O(4)#1	94.82(8)
N(3)–Ni(1)–O(1W)	94.45(9)	O(1)–Ni(1)–O(3)#1	106.65(8)
O(1)–Ni(1)–N(1)	88.30(8)	N(3)–Ni(1)–O(3)#1	158.28(8)
N(3)–Ni(1)–N(1)	90.68(9)	O(1W)–Ni(1)–O(3)#1	83.63(8)
O(1W)–Ni(1)–N(1)	174.53(9)	N(1)–Ni(1)–O(3)#1	92.31(8)
O(1)–Ni(1)–O(4)#1	166.81(8)	O(4)#1–Ni(1)–O(3)#1	60.47(7)
N(3)–Ni(1)–O(4)#1	97.84(8)		

Symmetry code: #1 *x*, –*y* + 2, *z* – 1/2

Table S6. Coordination modes of the **L** ligand and angle of two carboxyl groups of the aromatic polycarboxylates in complexes **1**–**5**.

Complex	**L**	Dihedral angle of two pyridyl rings (°)	Ni···Ni lengths (Å)	Aromatic polycarboxylate	Angle of two carboxyl groups (°)
1		0	22.15		180
2	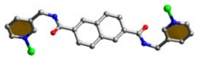	0	15.99		180
	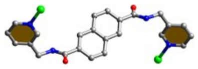	0	15.59		
3	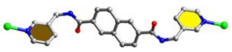	0	21.48	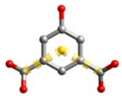	120
4	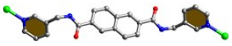	0	22.60	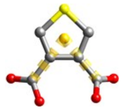	75
	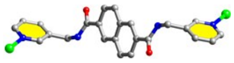	0	17.54		
5	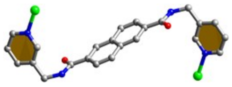	0	14.18	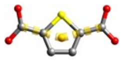	150
	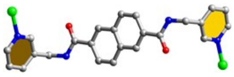	0	16.39		

Table S7. Selected hydrogen-bonding geometry (Å, °) for complexes **1–5**

Complex	D–H···A	D–H	H···A	D···A	D–H···A	ARU	Type
1	O1W–H1WA···O2	0.85	2.40	2.7195(18)	103	1 – *x*, –*y*, 1 – *z*	Intra
	O1W–H1WB···O5	0.85	1.98	2.8236(16)	174	*x*, –1 + *y*, 1 + *z*	
	N2–H2A···O2	0.86	2.11	2.8236(16)	170	*x*, 1 + *y*, *z*	
	C4–H4A···O1W	0.93	2.56	3.431(2)	155	2 – *x*, –*y*, 1 – *z*	
	C5–H5A···O1	0.93	2.49	3.022(2)	117		Intra
	C12–H12A···O2	0.93	2.56	3.2540(19)	132	2 – *x*, 1 – *y*, –*z*	
2	O1W–H1WA···O6	0.85	2.16	2.957(3)	156	*x*, 1 + *y*, *z*	
	O1W–H1WB···O2	0.85	1.80	2.634(3)	167		Intra
	O2W–H2WA···O4	0.85	1.73	2.579(3)	175		Intra
	N3–H3A···O2	0.86	2.36	3.083(3)	142	*x*, –1 + *y*, *z*	
	O2W–H2WB···O6	0.85	2.42	3.070(3)	134	*x*, 1 + *y*, *z*	
	N4–H4B···O5	0.86	2.12	2.963(3)	166	*x*, –1/2 – *y*, –1/2 + *z*	
	C11–H11A···O3	0.93	2.44	2.934(3)	114		Intra
	C16–H16A···O5	0.97	2.42	2.780(3)	101		Intra
	C23–H23A···O1	0.93	2.56	3.014(3)	110		Intra
	C27–H27A···N4	0.93	2.51	2.875(3)	103		Intra
3	O1W–H1A···O4	0.90	1.91	2.794(6)	167	–1/2 + *x*, 3/2 – *y*, –1/2 + *z*	
	O1W–H1B···O1	0.90	2.59	2.958(6)	106	–*x*, 2 – *y*, 1 – *z*	
	O1W–H1B···O2	0.90	1.81	2.684(7)	163	–*x*, 2 – *y*, 1 – *z*	
	N2–H2···O2	0.86	2.29	3.112(8)	161	*x*, 2 – *y*, 1/2 + *z*	
	O3–H3A···O2	0.90	2.37	3.220(7)	158	*x*, –1 + *y*, *z*	
	C12–H12···O2	0.93	2.59	3.481(9)	161	1/2 – *x*, –3/2 + *y*, 3/2 – *z*	
	C15–H15···O3	0.93	2.21	3.142(10)	180	*x*, 1 + *y*, *z*	
4	O1W–H1WA···O3	0.85	1.94	2.778(4)	170	–*x*, –*y*, 1 – *z*	
	O1W–H1WB···O6	0.85	1.94	2.778(4)	170	–*x*, 1 – *y*, –*z*	
	O2W–H2WA···O4	0.85	1.89	2.667(5)	152	–*x*, –*y*, 1 – *z*	

	O2W–H2WA···O5W	0.85	2.55	3.119(6)	125	–*x*, –*y*, 1 – *z*	
	N3–H3A···O2	0.85	2.53	2.797(5)	100	–*x*, –*y*, –*z*	
	N4–H4B···O3W	0.86	2.08	2.922(5)	167		
	O3W–H3WA···O5W	0.86	2.19	2.981(6)	152	*x*, *y*, –1 + *z*	
	O3W–H3WB···O1	0.85	2.41	2.987(5)	126	–*x*, –*y*, –*z*	
	O4W–H4WA···O4	0.85	2.11	2.935(5)	163	1 – *x*, –*y*, 1 – *z*	
	O4W–H4WB···O5	0.85	1.94	2.747(5)	159	–*x*, 1 – *y*, –*z*	
	O5W–H5WA···O4W	0.85	1.93	2.782(5)	177		
	O5W–H5WB···O4W	0.85	1.92	2.752(5)	167	1 – *x*, –*y*, 1 –*z*	
	C5–H5A···O3W	0.85	2.30	2.959(6)	135		
	C11–H11A···O1	0.93	2.56	3.218(6)	128		Intra
	C12–H12B···O5	0.93	2.60	3.049(6)	110		Intra
	C19–H19A···O1W	0.97	2.42	2.764(6)	100		Intra
	C21–H21A···O6	0.93	2.47	2.991(6)	115		Intra
	C24–H24A···O2	0.93	2.59	3.264(6)	130	–*x*, –*y*, –*z*	
	C30–H30A···O6	0.97	2.41	3.370(6)	169	1 – *x*, 1 – *y*, –1 – *z*	Intra
5	O1W–H1WA···O3W	1.03	1.80	2.825(3)	172		
	O1W–H1WB···O2	0.73	2.09	2.710(3)	143		Intra
	N2–H2A···O3	0.86	2.14	2.968(4)	162	1/2 – *x*, 3/2 – *y*, 1 – *z*	
	O2W–H2WA···O4	0.95	1.92	2.851(3)	169	*x*, 2 – *y*, –1/2 + *z*	
	O2W–H2WB···O6	0.88	1.97	2.820(4)	163		
	N4–H4B···O2W	0.86	2.06	2.852(4)	152	*x*, 1 – *y*, 1/2 + *z*	
	O3W–H3WA···O5	0.8	2.01	2.794(3)	167	–*x*, *y*, 1/2 – *z*	
	C7–H7A···O1	0.93	2.32	2.899(4)	120		Intra
	C10–H10A···O6	0.93	2.48	3.181(4)	132		Intra
	C15–H15A···O3	0.93	2.30	3.226(4)	172	1/2 – *x*, 3/2 – *y*,1 – *z*	
	C18–H18A···O6	0.93	2.45	2.779(4)	101		Intra
	C19–H19A···O2W	0.93	2.56	3.474(4)	168		
	C23–H23A···O1	0.93	2.50	3.090(3)	122		Intra
	C23–H23A···N4	0.93	2.53	2.866(4)	102		Intra

C24–H24B···S1	0.97	2.86	3.827(3)	179	*x*, –1 + *y*, *z*	
C30–H30A···O5	0.93	2.44	2.773(3)	101		Intra

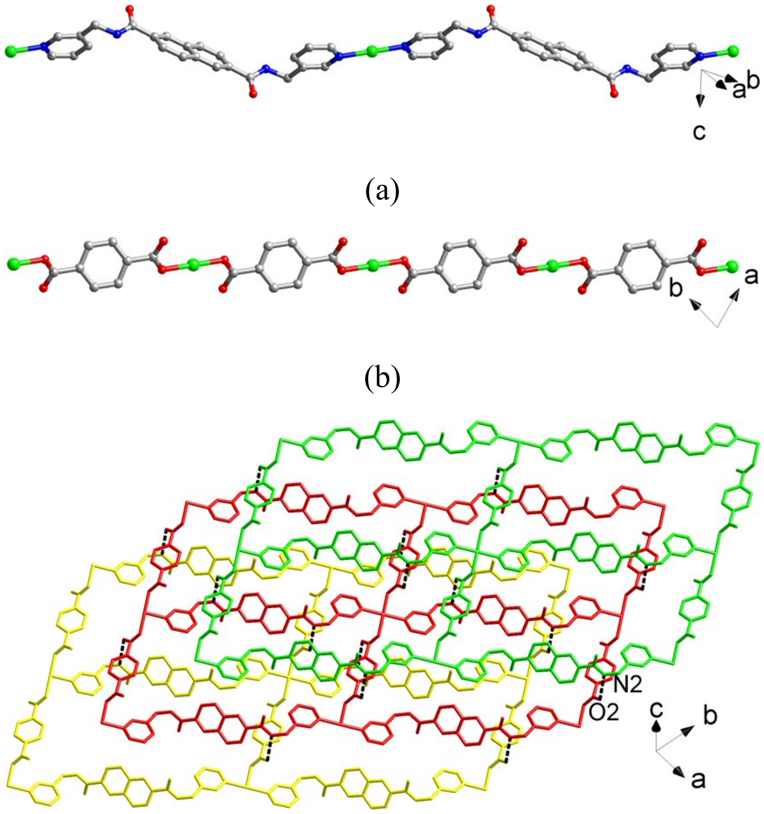

(a)

(b)

(c)

Fig. S1 (a) 1D [Ni-**L**]$_n$ chain in **1**; (b) 1D [Ni-(1,4-BDC)]$_n$ chain in **1**; (c) View of the 3D supramolecular framework of **1**.

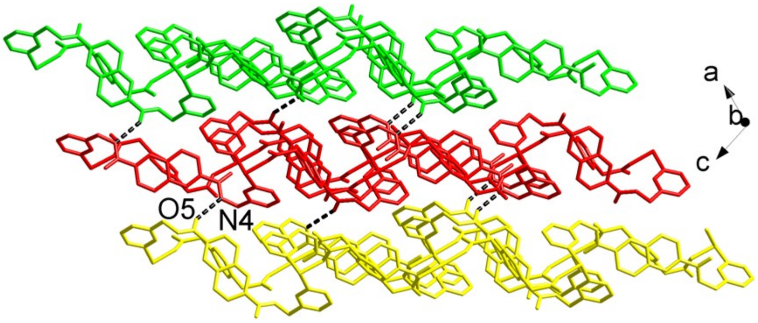

Fig. S2 View of the 3D supramolecular framework of **2**.

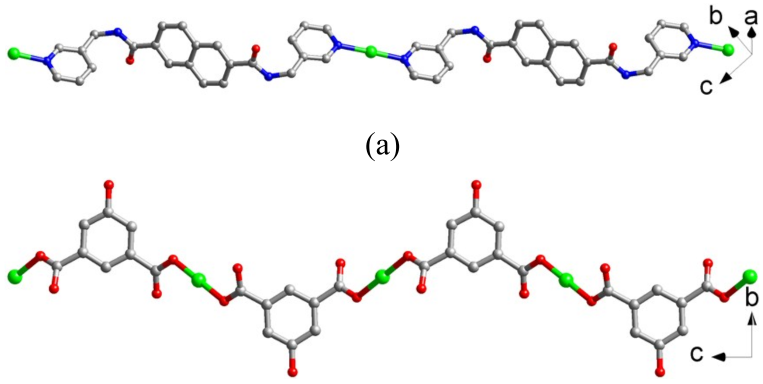

(a)

(b)

Fig. S3 (a) 1D [Ni−**L**]$_n$ chain in **3**; (b) 1D [Ni−(5-HIP)]$_n$ chain in **3**.

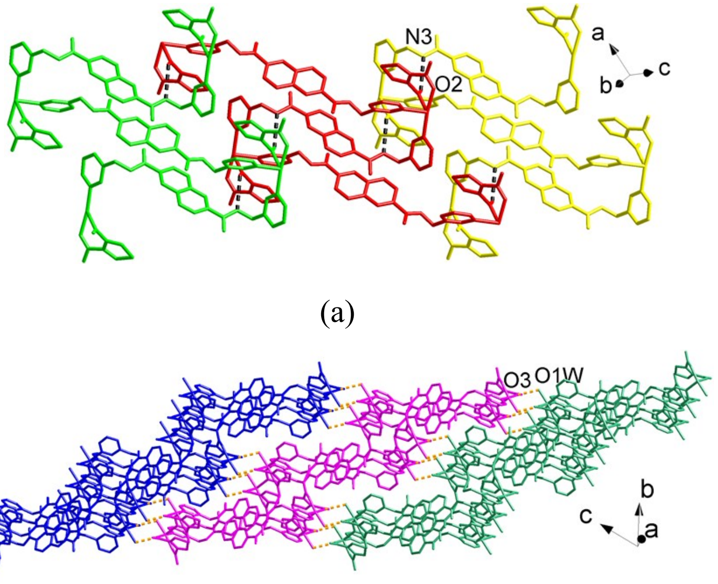

(a)

(b)

Fig. S4 (a) The 2D supramolecular network of **4**; (b) View of the 3D supramolecular framework of **4**.

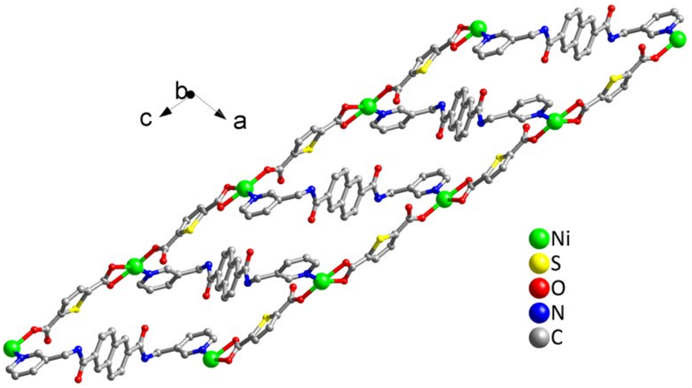

Fig. S5 The 1D ladder-like chain in complex **5**.

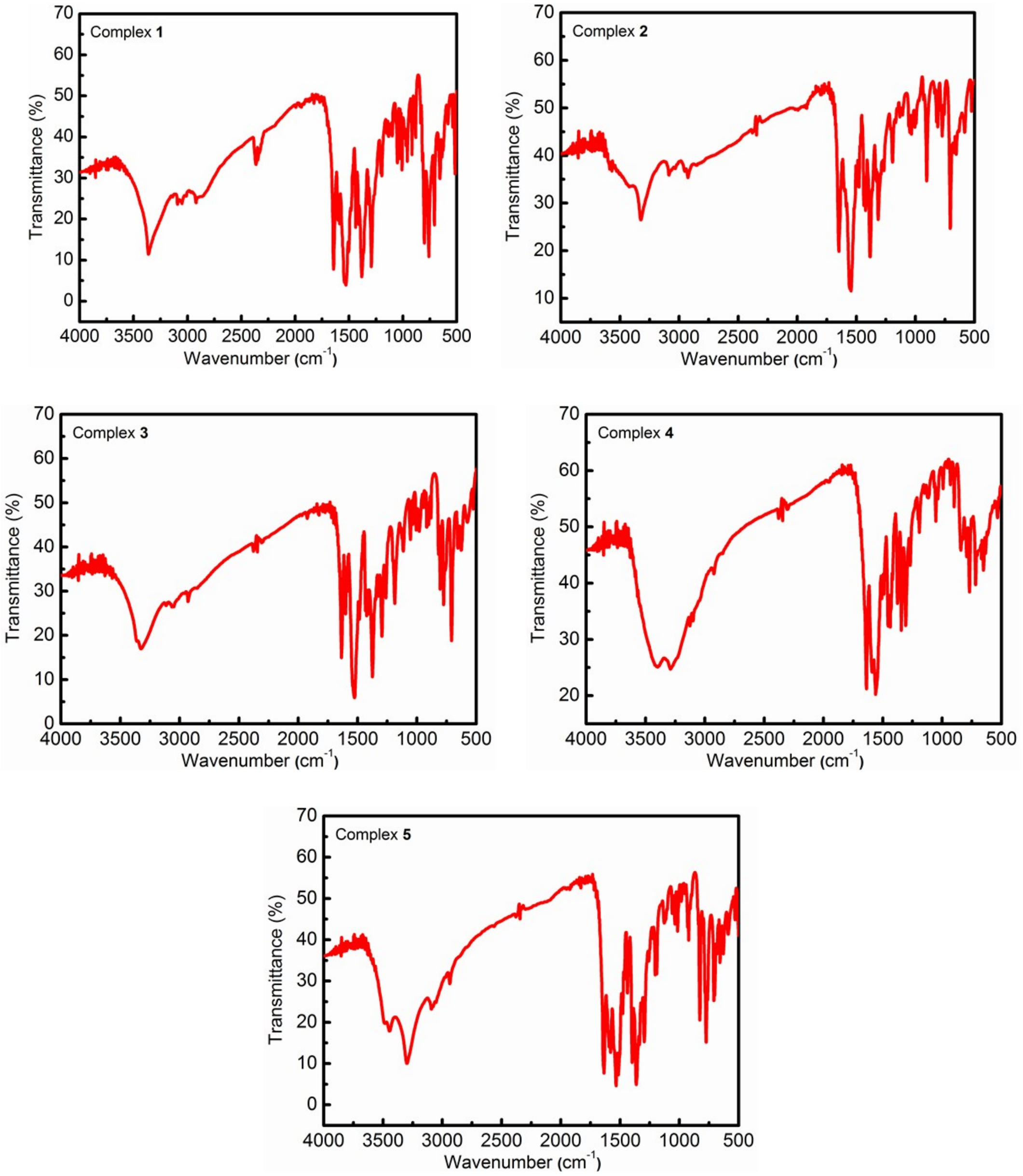

Fig. S6 The IR spectra of complexes **1**–**5**.

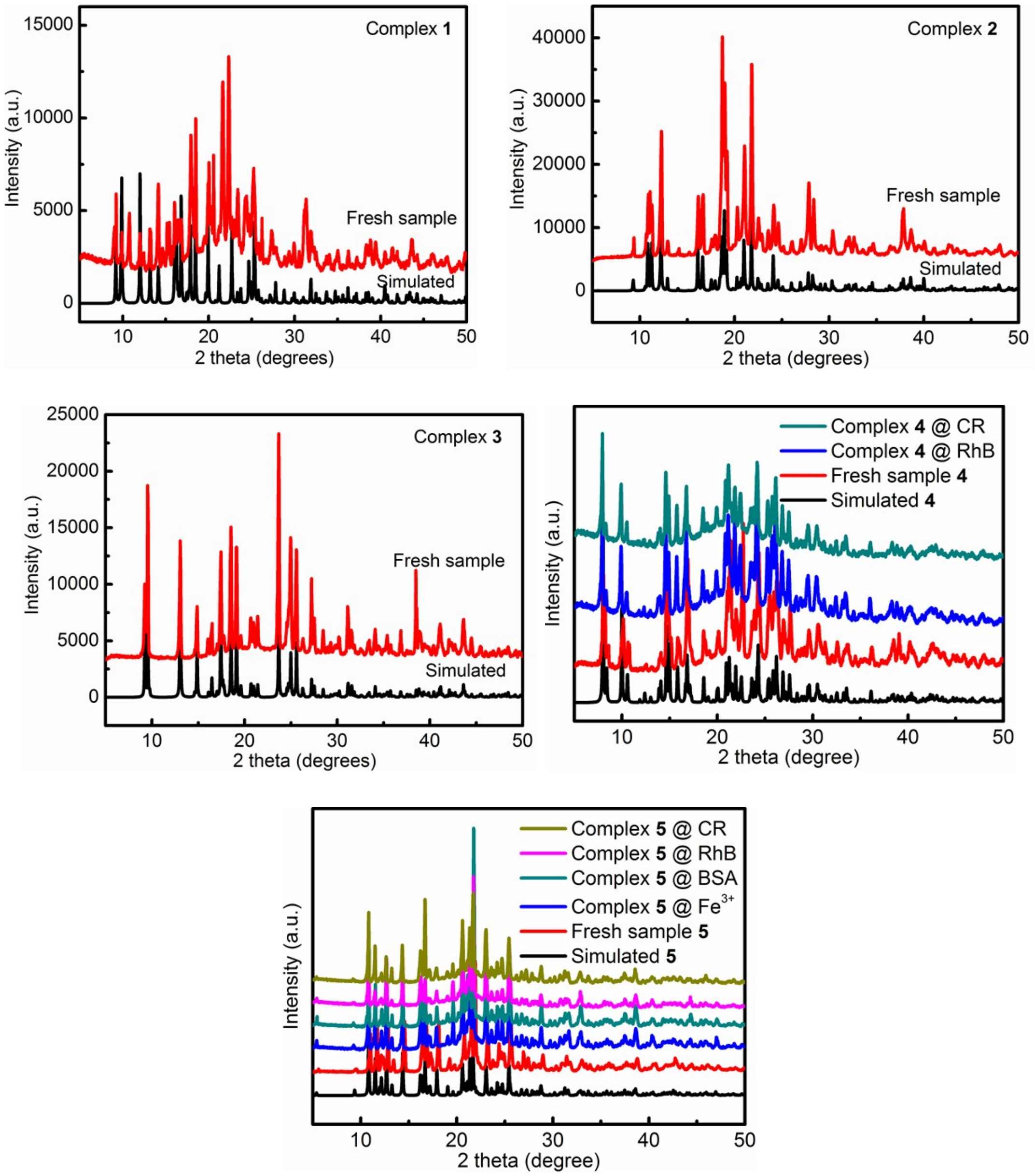

Fig. S7 The powder X–ray diffraction patterns of simulated, fresh samples and after the sensing and adsorption investigation for complexes **1**–**5**.

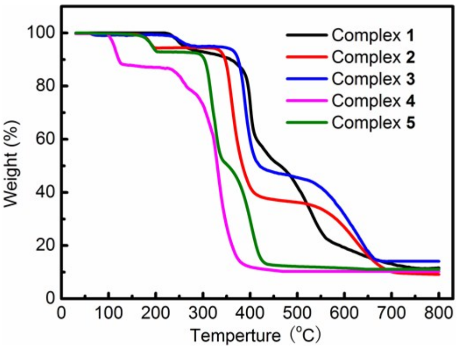

Fig. S8 The TG curves of complexes **1**–**5**.

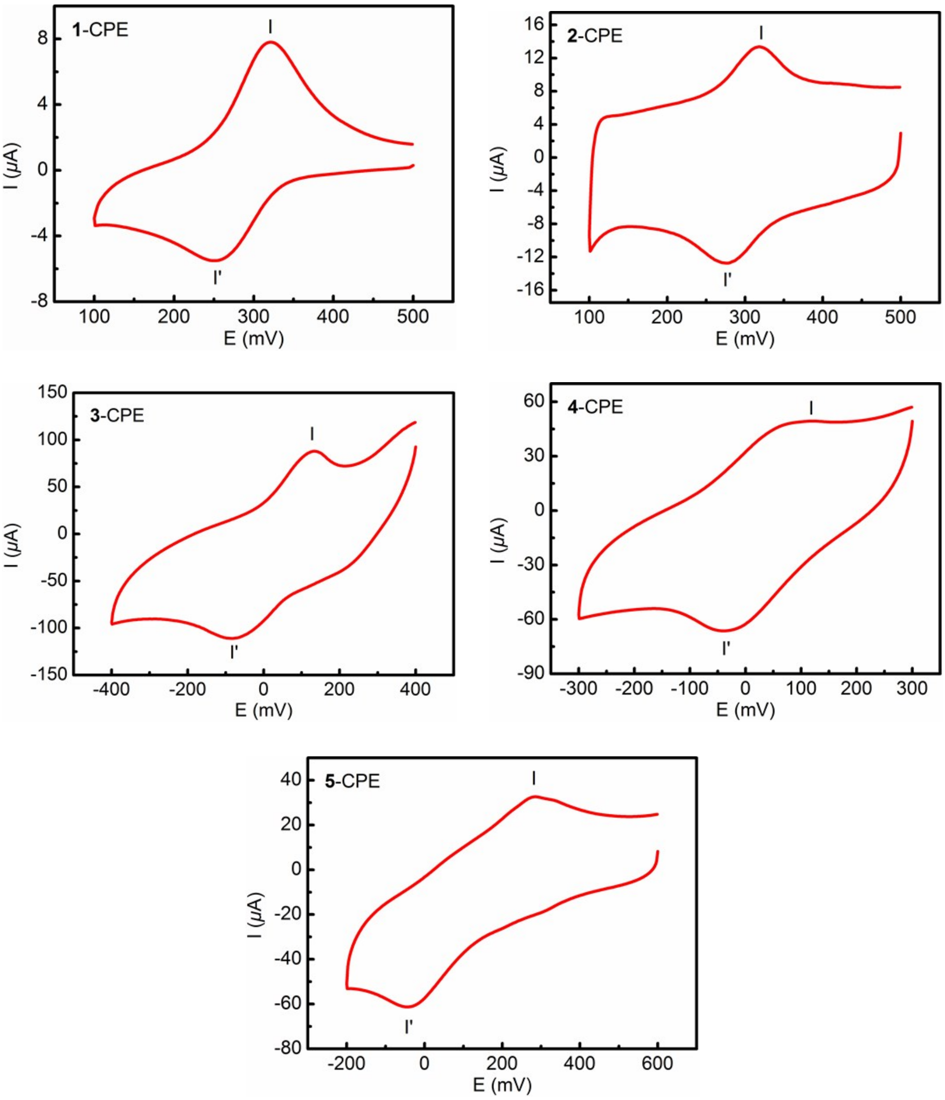

Fig. S9 Cyclic voltammograms of the **1**~**5**-CPEs in 0.1 M H_2SO_4 + 0.5 M Na_2SO_4

aqueous solution under scan rate of 140 mV s^{-1}.

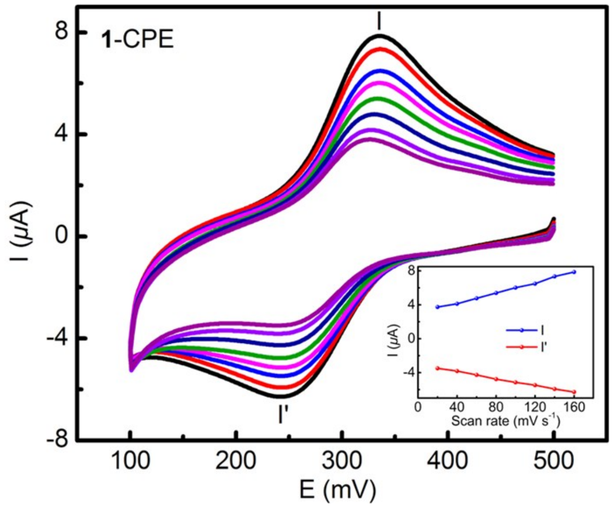

Fig. S10 Cyclic voltammograms of the **1**-CPE in 0.1 M H_2SO_4 + 0.5 M Na_2SO_4 aqueous solution under scan rates from inner to outer: (scan rates: 20, 40, 60, 80, 100, 120, 140 mV s^{-1}). Insert: the dependence of cathodic peak and anodic peak currents on scan rates of **1**-CPE.

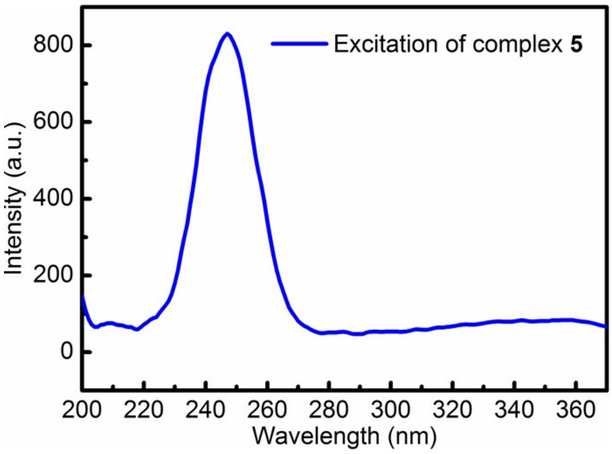

Fig. S11 The excitation spectrum of complex **5**.

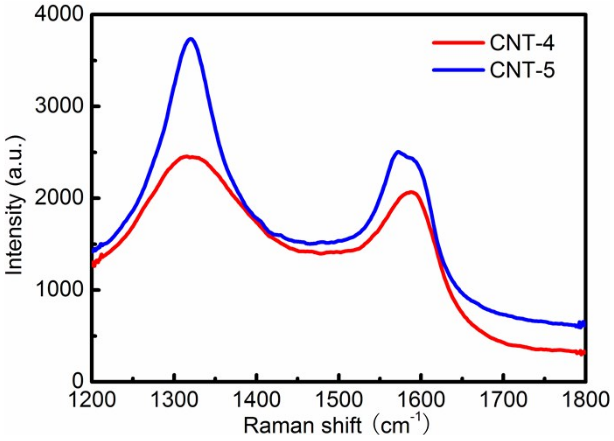

Fig. S12 Raman spectra of CNT-**4** and CNT-**5**.

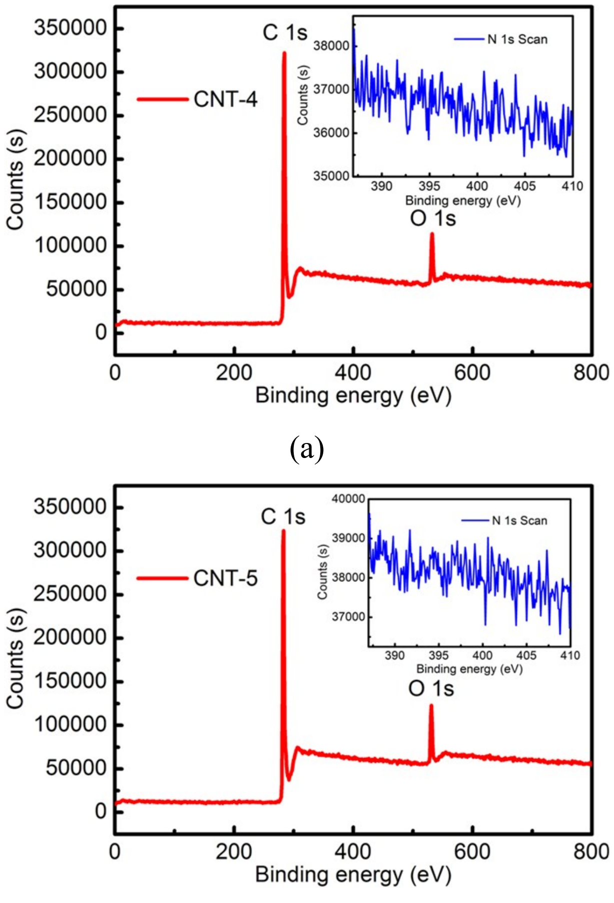

(a)

(b)

Fig. S13 XPS spectra of CNT-4 (a) and CNT-5 (b) (Inset: high-resolution details of the N 1s peaks).

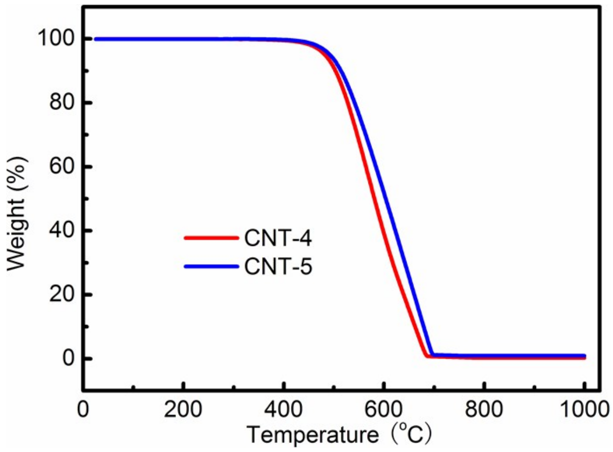

Fig. S14 TG curves of CNT-**4** and CNT-**5**.

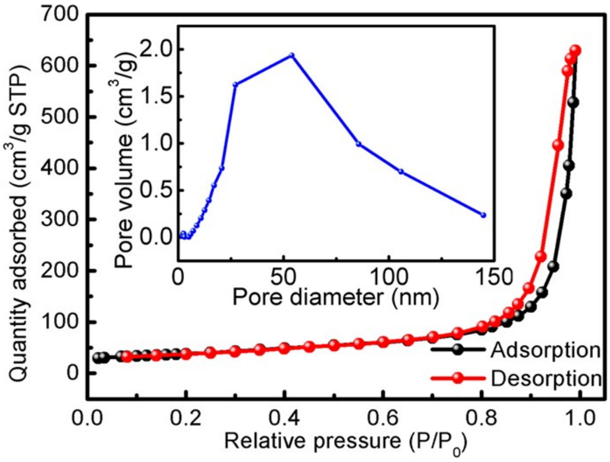

(a)

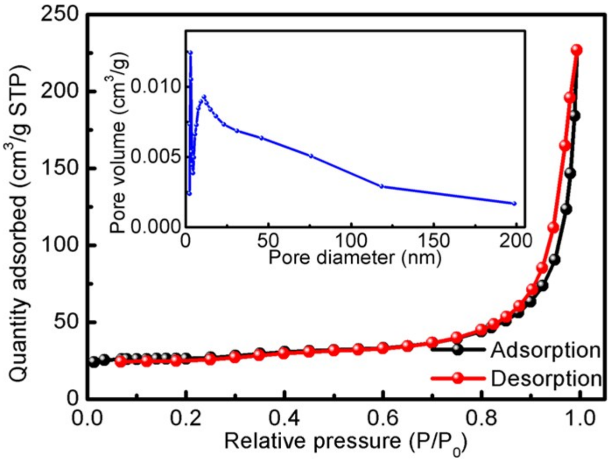

(b)

Fig. S15 Nitrogen adsorption and desorption isotherms of CNT-**4** (a) and CNT-**5** (b).

The inset shows the pore size distributions.

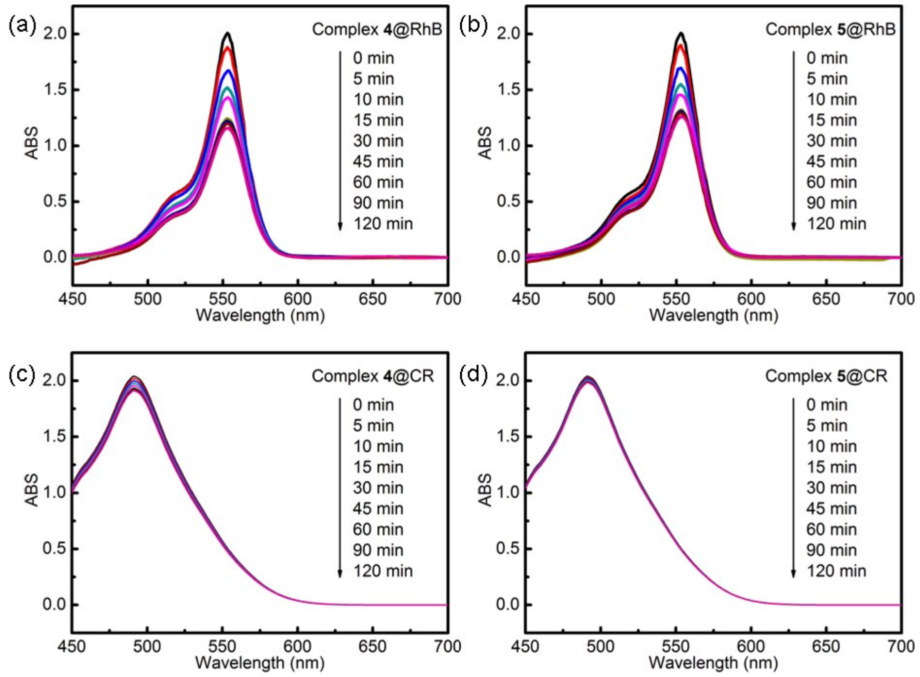

Fig. S16 (a) UV-vis spectra of RhB solution after different adsorption times with complex **4**; (b) UV-vis spectra of RhB solution after different adsorption times with complex **5**; (c) UV-vis spectra of CR solution after different adsorption times with complex **4**; (d) UV-vis spectra of CR solution after different adsorption times with complex **5**.

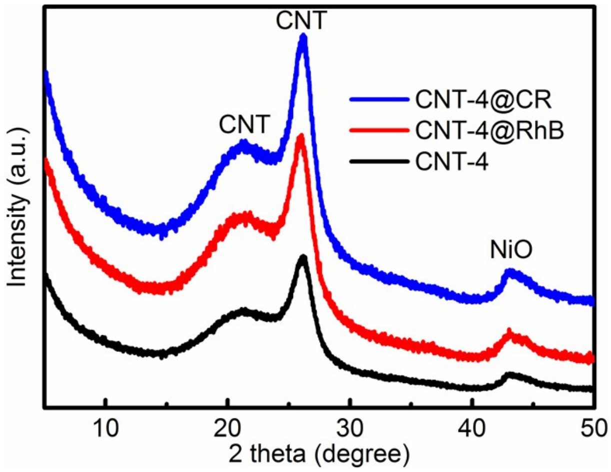

(a)

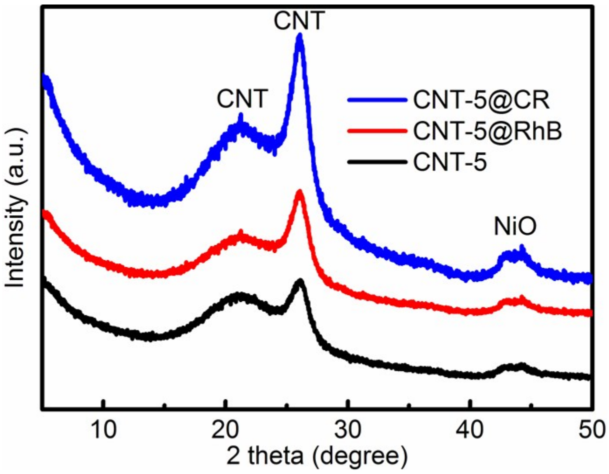

(b)

Fig. S17 The powder X–ray diffraction patterns of CNT samples and after the adsorption investigation for CNT-**4** and CNT-**5**.

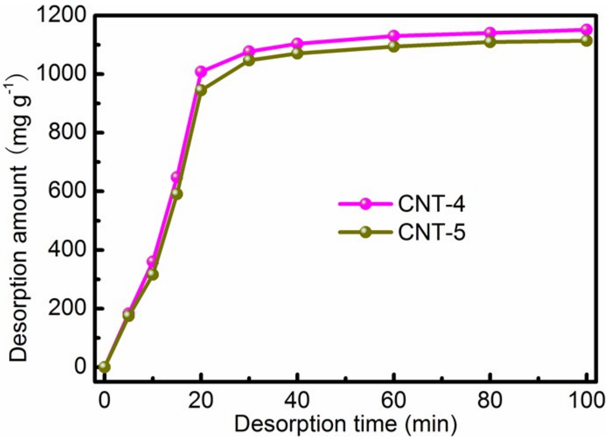

Fig. S18 The desorption amount of CR at different times with the CNTs.

References

[S1] M. Sarkar and K. Biradha, *Cryst. Growth Des.*, 2006, **6**, 202.

[S2] G. M. Sheldrick, *Acta Crystallogr., Sect. A: Found. Crystallogr.*, 2008, **64**, 112.

[S3] L. Y. Chen, J. F. Bai, C. Z. Wang, Y. Pan, M. Scheer and X. Z. You, *Chem. Commun.*, 2008, **13**, 1581.

[S4] W. Xia, A. Mahmood, R. Q. Zou and Q. Xu, *Energy Environ. Sci.*, 2015, **8**, 1837.

[S5] A. Mahmood, W. H. Guo, H. Tabassum and R. Q. Zou, *Adv. Energy Mater.*, 2016, **6**, 1600423.

[S6] J. S. Meng, C. J. Niu, L. H. Xu, J. T. Li, X. Liu, X. P. Wang, Y. Z. Wu, X. M. Xu, W. Y. Chen, Q. Li, Z. Z. Zhu, D. Y. Zhao and L. Q. Mai, *J. Am. Chem. Soc.*, 2017, **139**, 8212.

[S7] B. Y. Xia, Y. Yan, N. Li, H. B. Wu, X. W. Lou and X. Wang, *Nat. Energy*, 2016, **1**, 15006.

[S8] P. Pachfule, D. Shinde, M. Majumder and Q. Xu, *Nat. Chem.*, 2016, **8**, 718.